Ar_2 Photoelectron Spectroscopy Mediated by Autoionizing States

Marc Briant,[2,1] Lionel Poisson,[1,2,*] Majdi Hochlaf,[3] Patrick de Pujo,[2,1] Marc-André Gaveau,[2,1] and Benoît Soep[1,2]

[1]*Laboratoire Francis Perrin, CNRS, IRAMIS, SPAM, URA 2453, F-91191 Gif-sur-Yvette, France*
[2]*Laboratoire Francis Perrin, CEA, IRAMIS, SPAM, URA 2453, F-91191 Gif-sur-Yvette, France*
[3]*Laboratoire Modélisation et Simulation Multi-Echelle, MSME UMR 8208 CNRS, Université Paris-Est, 5 Boulevard Descartes, 77454 Marne-la-Vallée, France*

(Received 20 July 2012; published 9 November 2012)

This experimental work focuses on the complex autoionization dynamics of Ar_2 clusters below the first ionization energy of the argon atom. Ar_2 is submitted to vacuum ultraviolet radiation, and the photoelectron spectra are collected in coincidence with the cluster ions. The ionization dynamics is revealed by the dependence on the photon energy. We applied a new experimental method which we developed to analyze the photoelectron signal. Thus, we were able (i) to get the complete vibrational progression of Ar_2^+ that was never observed up to now, especially identifying the 0-0 transition overcoming the usual Franck-Condon limitations during single photoionization, and (ii) to obtain the projections of the vibrational wave functions of the autoionizing states over the Ar_2^+ functions. This method provides a powerful tool to test the potential energy curves computed by high level theoretical calculations on Rydberg states.

DOI: 10.1103/PhysRevLett.109.193401 PACS numbers: 36.40.−c, 32.80.Zb, 33.20.Tp, 33.60.+q

The chemistry of the interstellar medium [1] and that of planetary atmospheres such as that of Titan [2] are controlled by a network of ion-molecule reactions. An important issue in reaction dynamics is to develop strategies for their detailed understanding. Among these strategies, the threshold photoelectron photoion coincidence (TPEPICO) technique allows us either to prepare the ionic reactants with a well defined internal energy [3] or to explore the reactive surface when initiating the ion-molecule reaction [4] by ionization of a van der Waals complex between two neutral molecules. The latter approach and its variant, the pulsed field ionization-zero energy kinetic energy (PFI-ZEKE) method, have been also widely used for spectroscopic studies in small molecules [5]. The common and severe limitation of these techniques is the need to generate the ionic reactants with photoelectrons of nearly zero kinetic energy. In the PFI-ZEKE method, Rydberg states are populated and followed by a pulsed field ionization. The lifetime of the autoionizing Rydberg states populated should be sufficiently long [6] to allow delayed field ionization. In addition, slow electrons may not be easy to detect. This limits the number of systems that can be studied by these techniques. The present work bypasses these limitations by introducing a novel method which takes advantage of coincidence measurements between photoions and *nonzero* kinetic energy photoelectrons. We call this method SPES for slow photoelectron spectroscopy. In Ref. [7], an application of this method to the spectroscopy of biomolecules is already given. Here we show that the new method is a versatile alternative to TPEPICO and PFI-ZEKE and applicable when the two other fail. For instance, this happens frequently when the autoionizing intermediates have a short lifetime. Taking the well documented Ar^+-Ar system as a benchmark, the SPES method is applied here to show its capacity to explore quantitatively the shape of an ionic potential energy curve (PEC). In turn, from a fundamental point of view, the neutral argon dimer represents a model system which is weakly bound due to dispersive or inductive forces. Supersonic expansion allows its formation with the narrowest energy distribution. Its electronic excitation is accompanied by the formation of a strong bond with a large covalency character with *a priori* quite different contributions in the excited and in the ground ionic states. Because of the difference in equilibrium distances between the neutral ground state and the ionic ground state, the direct ionization process is strongly unfavored to nonrepulsive states, and a large range of energies is covered by the absorption of highly excited neutral Rydberg states subject to autoionization. By the way, such a situation is more general than the case of the Ar_2 system. It is met systematically when a pair of neutral identical molecules forms a complex bound by van der Waals forces. In such a case, the removal of an electron opens the possibility of a covalent bond, as here in Ar_2^+.

Up to now, the bond formation or breaking of van der Waals dimers, like $Ar_2^\star$ or Ar_2^+, has been studied mostly by the calculation of potential energy curves of the excimer [8] or of the ion [9–12]. Experiments were conducted to investigate the PEC of the excimer directly [13] or via the spectroscopy of Ar_2^* from $a^3\Sigma^+$ [14] or that of the ion by HeI photoelectron spectroscopy [15]. More accurate experiments were done to get the Ar_2^+ ground state vibrations by means of threshold photoelectron spectroscopy

[16]. The high-resolution PFI-ZEKE spectrum of Ar_2 and its isotopomer was used to extrapolate the location of the lowest vibrational level [17].

In the present Letter, we detect the Ar_2^+ vibrational bands up to the dissociation limit. Especially the origin band ν_0^+ of $Ar_2^+ \leftarrow Ar_2$ is directly measured for the first time. This is an illustration of the power of the SPES method to overcome the limitations of TPEPICO and PFI-ZEKE. These results are supported by a new set of state-of-the-art theoretical calculations on PECs of the lowest electronic states of the Ar_2^+ ion.

The experiments were performed on the DESIRS beam line [18] at the SOLEIL synchrotron, France (proposals No. 20080231, No. 20090200, and No. 20100366). We used the DELICIOUS II apparatus [19]. The synchrotron was used in the multibunch top-up mode at 400 mA.

The continuous argon beam mounted in the source chamber is based on a 50 μm nozzle cooled down by two Peltier modules (three-stage devices from Melcor, each one able to transfer a maximum of about 13 W of thermal power). The hot side of the modules was cooled by water at room temperature. The temperature of the source of the cluster is thus continuously tunable from 208 to 289 K. The pumping speed of the source chamber is 2900 $1 \cdot s^{-1}$. A mixture of 40% of argon in 60% of helium was used to avoid too large clustering. For a backing pressure of 4 bar and a temperature about 208 K, the cluster distribution observed by ionization in the range 14.55–14.65 eV did not show any significant population of $Ar_{n\geq 3}$ The dissociation energy of $Ar_3 + h\nu \rightarrow Ar_2^+ + Ar$ was calculated as 0.229 eV [20]. Below 14.68 eV, Ar_3 is also expected to remain unfragmented and to appear at mass 120.

The molecular beam enters the analysis chamber through a 1 mm skimmer. The PEPICO spectrometer DELICIOUS II used was described elsewhere [19]. Briefly, it couples a delay-line photoelectron velocity map imaging device [21] in coincidence with a standard time-of-flight mass spectrometer. Basically, an arriving electron on the delay line is spatially localized and starts the clock of the time-of-flight. The position of the detected electron is saved with the arrival time of its ion. This serves to reconstruct the spatial distribution of the electrons.

For these experiments, we used a moderate resolution using the high flux 200 grooves per mm grating, giving a typical bandwidth of about 2.5 meV. The resolution is resulting from the slit sizes of the monochromator. The photon flux was monitored thanks to a vacuum ultraviolet photodiode (IRD AXUV100). No gas filter was used for this experiment, since the grating suppresses most of the higher orders, even the second harmonic wavelength. In the present experiment the extraction voltage was set to 18 $V \cdot cm^{-1}$. With this extraction field, a 100% collection efficiency is guaranteed only for photoelectron kinetic energies below 190 meV. The redshift due to the extraction field, for this value, is estimated as $E_c = -3.2$ meV [22]. This applies only to the levels of the ion, since the autoionizing states energies are not affected by this shift [23]. Consequently, the electron yield is unchanged while the electron energy is shifted and the SPES spectrum is corrected by this amount.

In this Letter, we will focus on the signal collected in the 14.53–15.73 eV photon energy range, below the IE of the argon atom (ionization energy: 15.759 606 eV [24]) as well as that of helium (24.58 741 eV). The energy range from 14.53 to 15.73 eV was cut into several ranges and sampled by steps of 0.75 or 0.5 meV depending on the state density. The slits size, as well as the integration time, was adjusted depending on the signal flux, which was normalized on the integrated photon flux. The following results were collected by selecting only the events giving an Ar_2^+ ion. The monochromator was calibrated on the ionization threshold of N_2 and resonances of O_2, which are occurring in the 14.53–15.73 eV range, to allow the precise overlap of the separate scans. False coincidences were subtracted. For each photon energy, the photoelectron spectrum obtained is inverted by using the polar basis function expansion procedure [25] with a basis set including P_0 and P_2 contributions. This mathematical inversion provides the cut of the Newton sphere which is projected on the detector: It removes also the electrons of high energy ejected toward the detector but induces some noise in the few center pixels, of computation origin. No significant polarization in the electron emission was measured. Then, only the total signal distribution P_0 will be presented.

Figure 1 presents the SPES matrix. See Ref. [7] for a detailed description of this data treatment. Briefly, the matrix shows the photoelectron spectrum (vertical axis) for each photon energy. The vertical summation of the matrix gives the electron yield (presented in blue on the bottom of Fig. 1). It is the action spectrum for the formation of Ar_2^+. Below the vertical direct ionization threshold [15], the structures represent the autoionization resonances, and they are part of the Ar_2 absorption spectrum. The white diagonal lines correspond to constant ion

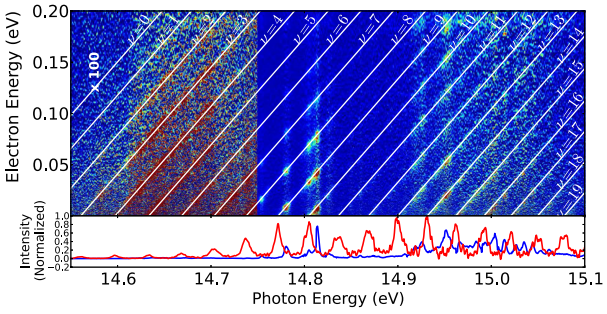

FIG. 1 (color online). (Top) Selection on the 2D SPES matrix. Intensities are mapped from blue to red. (Bottom) SPES spectrum [red (light) line] and electron yield [blue (dark) line] vs the photon energy.

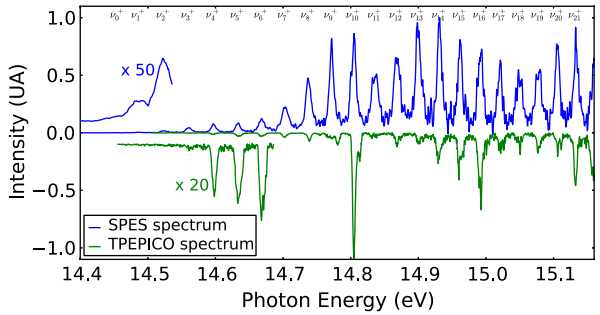

FIG. 2 (color online). The SPES spectrum is compared to the TPEPICO spectrum. Both are derived from the present same set of experimental data.

energies: The photon energy minus electron energy is a constant. In order to get the SPES spectrum, the matrix is summed along the direction of these white lines; i.e., the pixel intensities are summed along these lines. The corresponding spectrum is presented as the red curve in Fig. 1. We limited here the projection to electrons with energies below 170 meV. The major improvement of the SPES method is the detection of vibrational levels even if there is no absorption at the energy of the vibrational level. As shown in Figs. 1 and 2, the vibrational levels ν_0^+, ν_1^+, ν_2^+, and ν_4^+ as well as ν_{11}^+ are observed without any difficulty, which is definitely not the case for either the conventional TPEPICO [16] (Fig. 2) or the ZEKE-PFI methods [17]. One can notice in Fig. 1 that the lowest vibrational levels, such as the ν_0^+ state, are observed far from their threshold energy. The SPES treatment is therefore a powerful tool to get around the Franck-Condon spectral limitations. Furthermore, SPES shows a clearly better signal-to-noise ratio than TPEPICO as can be observed in Fig. 2, which represents the SPES and the TPEPICO spectra over the same experimental data.

The SPES spectrum was fitted by a bunch of Gaussian functions, up to the 53rd vibration level (see Fig. 3). For each band, a superposition of two Gaussian functions with the same energy origin, but with different full widths at half maximum (6.5 and 23 meV), was used to fit the shape of

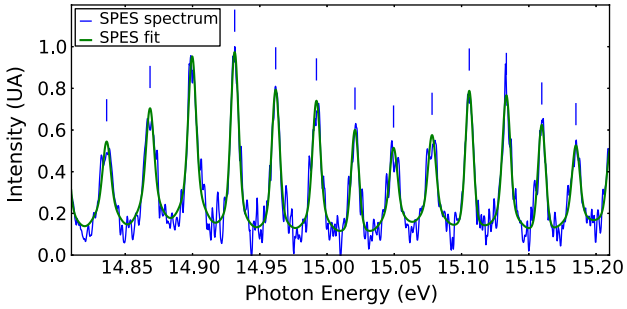

FIG. 3 (color online). The SPES spectrum and the synthetic spectrum using a fit of the vibrational progression by a sum of Gaussian functions.

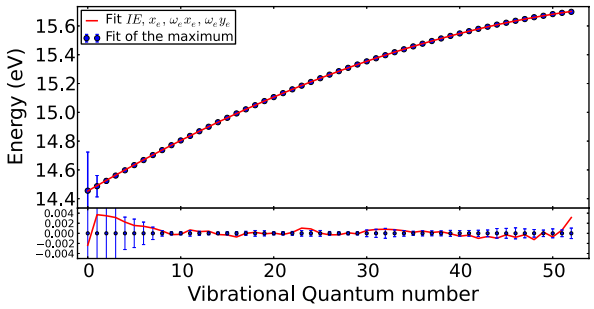

FIG. 4 (color online). Upper trace: Energy and error bar measured as the function of the vibrational quantum number. The fit of the progression is plotted. Lower trace: Standard deviation for each experimental peak energy (errorbars) and the difference between the experimental peak energies and the position of peaks given by the fit.

the SPES structure. All intensities and band origins were fitted simultaneously, with a total of 159 parameters. The band energies as well as their corresponding standard deviation were used to fit the vibrational progression. The fitting function is of the form $E(\nu) = \mathrm{IE} + \omega_e(\nu+1/2) - \omega_e x_e(\nu+1/2)^2 + \omega_e y_e(\nu+1/2)^3 - \omega_e/2 + \omega_e x_e/4 - \omega_e y_e/8$ (see Fig. 4), where the spectroscopic constants describe the Ar_2^+ ground state PEC. From these spectroscopic constants we reconstructed the RKR PEC [26] (see Fig. 5). The resulting curve nicely matches the PEC calculated by Merkt's group [12] and fitted by Bonhommeau, Halberstadt, and Viel [11].

We list in Table I the IE, the harmonic (ω_e), the anharmonic terms ($\omega_e x_e$ and $\omega_e y_e$), and the dissociation energy (D_0) of Ar_2^+ $X^2\Pi_u$ deduced from our fitting procedure. We give also those of Refs. [16,17] for comparison. We notice

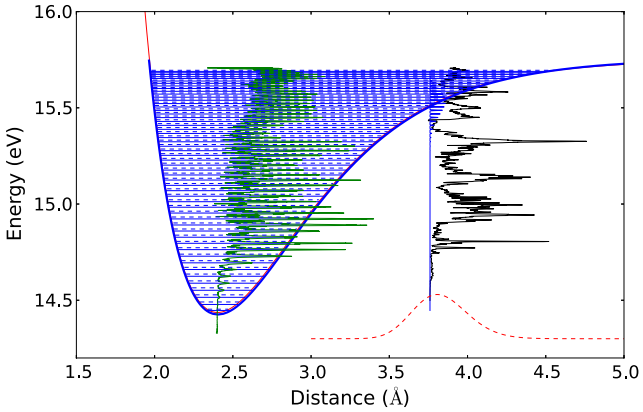

FIG. 5 (color online). Black: Electron yield (autoionizing resonances); green (light): SPES spectrum; blue (dark): RKR reconstructed PEC. Red dashed line: Wave function of the ground state $\nu = 0$ of Ar_2. Thin red line: PEC calculated at internally contracted multi reference configuration interaction including Davidson correction level with the aug-cc-pV6Z basis set and basis set superposition error correction at the coupled cluster approach with perturbative treatment of triple excitations level.

TABLE I. Spectroscopic parameters of the ground electronic state of Ar_2^+ deduced from the fit of the vibrational progression.

IE (eV)	ω_e (meV)	$\omega_e x_e$ (meV)	$\omega_e y_e$ (μeV)	D_0 (eV)	Reference
14.450 ± 0.005	39.0 ± 0.1	0.283 ± 0.002	···	1.320 ± 0.005	[16][a]
14.4558 ± 0.0007	38.06 ± 0.05	0.254 ± 0.006	···	1.3144 ± 0.0007	[17]
14.4564 ± 0.0008	37.7 ± 0.1	0.233 ± 0.004	−0.50 ± 0.05	1.3136 ± 0.0008	This work experimental
14.4645 ± 0.0002	37.81 ± 0.02	0.235 ± 0.001	−0.52 ± 0.01	1.3056 ± 0.0002	This work calculation

[a]Assuming the first level observed is $\nu^+ = 3$.

that the standard deviation is quite good. All energies issued from the best fit are within the vibration levels range given by their standard deviation (see Fig. 4). The main results we obtained are (i) the ν_0^+ is directly observable thanks to the SPES method and is compatible with the value given here—besides this level is located outside the Ar_2 Franck-Condon zone, (ii) an accurate IE of Ar_2 is directly determined; and (iii) this allows the accurate measurement of the high vibration levels of Ar_2^+. The position in energy of these bands is sensitive to the shape of the PEC close to dissociation and to the close-lying and possibly interacting states. Figure 5 shows also the computed *ab initio* PEC, using the internally contracted multi reference configuration interaction including Davidson correction method [27–29] with basis set superposition error correction [calculated with the coupled cluster approach with perturbative treatment of triple excitations method [30–32] to avoid size consistency problems] and the aug-cc-pV6Z basis set + SO + DK [33]. It can be seen there that we have a good agreement between the curves above 3 Å. In Table I are reported the harmonic and anharmonic terms deduced from a Numerov-Cooley [34] Hamiltonian integration of the calculated PEC. The fitting parameters confirm that the shape of the PEC is very close to the experimental one. Standard deviations are due to the lack of correspondence between the Dunham coefficients and the ''true'' curves. It gives the experimental limitation for spectra without rotational resolution. However, the RKR potential slightly deviates from the *ab initio* one, close to the minimum, despite the large size of these computations. This discrepancy comes most likely from the impossibility of the state-of-the-art basis set used to describe accurately the Ar atom at large internuclear distances and to fully consider its relativistic effects. This work should motivate new theoretical developments in this direction.

The fitting of the vibrational progression gives an energy and an assignment for each white line of Fig. 1. For a given photon energy, i.e., a given autoionization band, the signal spots appearing for each Ar_2^+ vibrational level yield its weight in the vibrational distribution. This relative distribution can be modelized by the direct projection of the vibrational wave function initially populated in the autoionizing state $Ar_2^\star$ on the low-lying vibrational states of Ar_2^+. These wave functions can be constructed based on a Numerov-Cooley [34] integration of the RKR potential energy curve. One can try to reconstruct the overlapping part of the initially populated vibrational wave function of $Ar_2^\star$, by using the coefficients obtained by the SPES analysis. The projection remains, however, uncomplete, since the whole Franck-Condon projection is not available because of energetic considerations. This procedure is a kind of reverse serial Fourier transform, but with only a small set of coefficients and especially not necessarily the most relevant ones.

Interestingly, these accurate experimental data can be useful to test the reliability of the calculated potential energy curves of the autoionizing excited argon dimer. Indeed, one can extract some qualitative information. For example, the autoionizing resonance at 14.960 eV (Fig. 1) shows the coefficient go down from $\nu^+ = 13$ to $\nu^+ = 12$ and then rise starting from $\nu^+ = 10$. This suggests some complexity of potential energy curves compared to the other resonances. As already mentioned, the projection acts as a serial Fourier transform, since the local oscillation period of the wave function depends at a given distance on the momentum. This is why the excited $Ar_2^\star$ couples to vibrational levels of Ar_2^+ having locally the same spatial oscillation period, i.e., overlap at least partially with the same momentum. To the best of our knowledge, this is the first direct measurement of such an effect.

In the present Letter, we were able to observe experimentally the whole set of vibrational levels of Ar_2^+ and to reconstruct accurately its PEC. We measured the projection of the vibrational wave function of the excited states to the lower-lying ionic ones. These results can be used to test accurately calculated potential energy curves of highly excited $Ar_2^\star$. This method can be extrapolated to other bimolecular systems and furnish accurate data to theoreticians interested in dissociative electron recombination. Generally, it can be applied to homonuclear diatomic molecules as well as heteronuclear ones where the PEC can be even more complex. Applying such a method to compounds of atmospheric interest such as N_2^+ or NO^+ and other compounds of interest should clearly help in the understanding of their behavior at high layers of the atmosphere. Furthermore, the complex photoionization dynamics revealed by the present experimental work, where non–Born-Oppenheimer effects are obviously in action, should be investigated deeply by new theoretical approaches such as those developed, for instance, by Greene and Jungen [35].

We are grateful to Dr. Gustavo Garcia for assistance and to the SOLEIL staff for smoothly running the facility. We thank Dr. Laurent Nahon, DESIRS beam line director. We are grateful to Dr. Antoine Masson, Dr. Giovanni Piani, and Dr. Jean-Michel Mestdagh for their help during the acquisition of the data.

*lionel.poisson@cea.fr

[1] W. Klemperer, Annu. Rev. Phys. Chem. **62**, 173 (2011).
[2] A. J. Coates, J. E. Wahlund, K. Agren, N. Edberg, J. Cui, A. Wellbrock, and K. Szego, Space Sci. Rev. **162**, 85 (2011).
[3] H. Palm, C. Alcaraz, P. Millié, and O. Dutuit, Int. J. Mass Spectrom. **249–250**, 31 (2006).
[4] S. Martrenchard, C. Dedonder-Lardeux, I. Dimicoli, G. Grégoire, C. Jouvet, M. Mons, and D. Solgadi, Chem. Phys. **239**, 331 (1998).
[5] L. Piticco, M. Schaefer, and F. Merkt, J. Chem. Phys. **136**, 074 304 (2012).
[6] F. Merkt, R. J. Rednall, S. R. Mackenzie, and T. P. Softley, Phys. Rev. Lett. **76**, 3526 (1996).
[7] J. C. Poully, J. P. Schermann, N. Nieuwjaer, F. Lecomte, G. Grégoire, C. Desfrancois, G. A. Garcia, L. Nahon, D. Nandi, L. Poisson, and M. Hochlaf, Phys. Chem. Chem. Phys. **12**, 3566 (2010).
[8] P. Duplaa and F. Spiegelmann, J. Chem. Phys. **105**, 1500 (1996).
[9] F. X. Gadea and I. Paidarová, Chem. Phys. **209**, 281 (1996).
[10] A. Wuest and F. Merkt, J. Chem. Phys. **120**, 638 (2004).
[11] D. Bonhommeau, N. Halberstadt, and A. Viel, J. Chem. Phys. **124**, 184314 (2006).
[12] T. K. Ha, P. Rupper, A. Wuest, and F. Merkt, Mol. Phys. **101**, 827 (2003).
[13] Y. Tanaka and K. Yoshino, J. Chem. Phys. **53**, 2012 (1970).
[14] D. J. Kane, S. B. Kim, D. C. Shannon, C. M. Herring, J. G. Eden, and M. L. Ginter, J. Chem. Phys. **96**, 6407 (1992).
[15] T. Pradeep, B. Niu, and D. A. Shirley, J. Chem. Phys. **98**, 5269 (1993).
[16] R. I. Hall, Y. Lu, Y. Morioka, T. Matsui, T. Tanaka, H. Yoshii, T. Hayaishi, and K. Ito, J. Phys. B **28**, 2435 (1995).
[17] R. Signorell, A. Wuest, and F. Merkt, J. Chem. Phys. **107**, 10 819 (1997).
[18] L. Nahon, N. de Oliveira, G. A. Garcia, J.-F. Gil, B. Pilette, O. Marcouille, B. Lagarde, and F. Polack, J. Synchrotron Radiat. **19**, 508 (2012).
[19] G. A. Garcia, H. Soldi-Lose, and L. Nahon, Rev. Sci. Instrum. **80**, 023 102 (2009).
[20] D. Hrivňák and R. Kalus, Chem. Phys. **264**, 319 (2001).
[21] A. Eppink and D. H. Parker, Rev. Sci. Instrum. **68**, 3477 (1997).
[22] C. Bordas, Phys. Rev. A **58**, 400 (1998).
[23] H. H. Fielding and T. P. Softley, J. Phys. B **25**, 4125 (1992).
[24] I. Velchev, W. Hogervorst, and W. Ubachs, J. Phys. B **32**, L511 (1999).
[25] G. A. Garcia, L. Nahon, and I. Powis, Rev. Sci. Instrum. **75**, 4989 (2004).
[26] R. J. Le Roy, *RKR1 2.0: A Computer Program Implementing the First-Order RKR Method for Determining Diatomic Molecule Potential Energy Curves*, Chemical Physics Research Report (University of Waterloo, Waterloo, 2004). The source code and manual for this program may be obtained from the Computer Programs link at http://leroy.uwaterloo.ca.
[27] P. J. Knowles and H. J. Werner, Chem. Phys. Lett. **145**, 514 (1988).
[28] H. J. Werner and P. J. Knowles, J. Chem. Phys. **89**, 5803 (1988).
[29] S. R. Langhoff and E. R. Davidson, Int. J. Quantum Chem. **8**, 61 (1974).
[30] P. J. Knowles, C. Hampel, and H. J. Werner, J. Chem. Phys. **99**, 5219 (1993).
[31] P. J. Knowles, C. Hampel, and H. J. Werner, J. Chem. Phys. **112**, 3106 (2000).
[32] K. Raghavachari, G. W. Trucks, J. A. Pople, and M. Head-Gordon, Chem. Phys. Lett. **157**, 479 (1989).
[33] A. K. Wilson, T. van Mourik, and T. H. Dunning, J. Mol. Struct. **388**, 339 (1996).
[34] J. W. Cooley, Math. Comput. **15**, 363 (1961).
[35] C. H. Greene and C. Jungen, Adv. At. Mol. Phys. **21**, 51 (1985).